

Tunable sign change of spin Hall magnetoresistance in Pt/NiO/YIG structures

Dazhi Hou,^{1,2} Zhiyong Qiu,^{1,2,*} Joseph Barker,³ Koji Sato,¹ Kei Yamamoto,^{3,4,5} Saül Vélez,⁶ Juan M. Gomez-Perez,⁶ Luis E. Hueso,^{6,7} Fèlix Casanova,^{6,7} and Eiji Saitoh^{1,2,3,8}

¹WPI Advanced Institute for Materials Research, Tohoku University, Sendai 980-8577, Japan

²Spin Quantum Rectification Project, ERATO, Japan Science and Technology Agency, Sendai 980-8577, Japan

³Institute for Materials Research, Tohoku University, Sendai 980-8577, Japan

⁴Institut für Physik, Johannes Gutenberg Universität Mainz, D-55099 Mainz, Germany

⁵Department of Physics, Kobe University, 1-1 Rokkodai, Kobe 657-8501, Japan

⁶CIC nanoGUNE, 20018 Donostia-San Sebastian, Basque Country, Spain

⁷IKERBASQUE, Basque Foundation for Science, 48011 Bilbao, Basque Country, Spain

⁸Advanced Science Research Center, Japan Atomic Energy Agency, Tokai 319-1195, Japan

Spin Hall magnetoresistance (SMR) has been investigated in Pt/NiO/YIG structures in a wide temperature range. The SMR changes sign at a temperature which increases with the NiO thickness. This is contrary to a conventional SMR theory picture applied to Pt/YIG bilayer which always predicts a positive SMR. We explain the negative SMR at low temperatures by the NiO ‘spin-flop’ coupled with YIG, which is overridden at higher temperature by positive SMR contribution from YIG. This highlights the role of magnetic structure in antiferromagnets for transport of pure spin current in multilayers.

Magnetoresistance plays essential roles in providing both a fundamental understanding of electron transport in magnetic materials and in various technological applications. Anisotropic magnetoresistance (AMR) [1, 2], giant magnetoresistance [3, 4], and tunneling magnetoresistance [5–8] underpin technologies in sensors, memories, and data storage. Recent studies of thin film bilayer systems comprised of a normal metal (NM) and a ferromagnetic insulator (FI) revealed a new type of magnetoresistance called spin Hall magnetoresistance (SMR) [9–11], originating from the interplay between the spin accumulation at the NM/FI interface and the magnetization of the FI layer. When the NM layer has a significant spin-orbit interaction, e.g. Pt, an in-plane charge current \mathbf{j}_c induces a spin current via the spin Hall effect, which in turn generates a spin accumulation near the NM/FI interface. At the same time, this spin accumulation is affected by the orientation of the magnetization in the ferromagnet. The conductivity of the NM layer is thus subject to a magnetization dependent modification to the leading order in θ_{SHE}^2 , where θ_{SHE} is the spin Hall angle in the NM layer.

Since the discovery of SMR, experimental studies were instigated in various systems [12–19]. The amplitude of SMR is defined as the difference of the resistivities with an applied field, H , perpendicular (ρ_{\parallel}) and parallel (ρ_{\perp}) to \mathbf{j}_c : $\rho_{\text{SMR}} = \rho_{\parallel} - \rho_{\perp}$. This is predicted to be always positive because when $H \parallel \mathbf{j}_c$, the FI can absorb more spin current, by which the backflow required to ensure the stationary state is reduced at the FI/NM interface, in turn causing less secondary forward charge current, and therefore gives: $\rho_{\parallel} > \rho_{\perp}$ [9, 10]. Positive ρ_{SMR} is found in most experimental observations.

Very recently, a negative SMR ($\rho_{\parallel} < \rho_{\perp}$) was reported when an antiferromagnetic (AFM) insulator, in this case NiO, is inserted between Pt and YIG [20]. The negative

SMR was also found to revert to the conventional positive sign at higher temperatures. Signal contamination from other magnetoresistances such as AMR was excluded by a systematic field angle dependence measurement. This result challenges the present understanding of SMR. Since the SMR does not change its sign in the Pt/YIG bilayer structure, the NiO layer must be the cause. However, it is not clear why NiO should give a negative SMR since antiferromagnets are thought only to affect the efficiency of the spin communication between Pt and YIG [21–26].

In this letter, we report the temperature dependence of SMR in Pt/NiO/YIG structures with different thicknesses of NiO. The temperature at which the SMR becomes negative is found to depend on the NiO thickness. The anomalous negative SMR at low temperatures is explained from a ‘spin-flop’ configuration whereby the Néel order of the NiO is perpendicularly coupled to the magnetization of YIG [27]. As the spin conductivity of NiO increases with increasing temperature [24–26], the moments of the YIG beneath have an increasing influence on the total SMR signal. The positive SMR contribution from YIG competes the negative SMR from NiO. At the sign change, the competition leads to a vanishing SMR. Above, in the high temperature regime, the positive SMR of the YIG dominates. We introduce a phenomenological model to describe the competition between the positive and negative SMR contributions, which reproduces the NiO thickness dependent SMR sign change behaviors in Pt/NiO/YIG.

An epitaxial YIG film of thickness 3 μm was grown on a gadolinium gallium garnet (111) substrate prepared by the liquid phase epitaxy growth method. NiO films of different thicknesses were grown by sputtering onto the YIG surface at 400 °C. The film was then covered with 4 nm of sputtered Pt. Figure 1(a) shows the schematic illustration for the electric measurement setup: a magnetic field

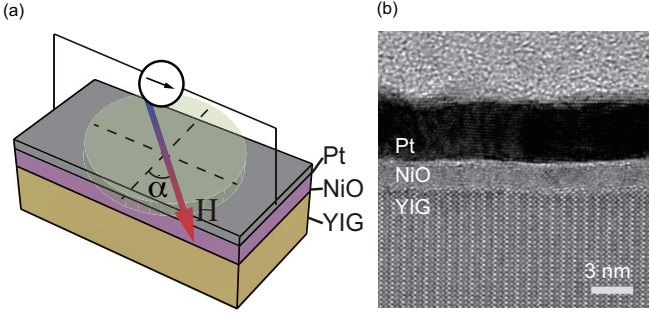


FIG. 1. (a) Illustration of the magnetoresistance measurement setup for the Pt/NiO/YIG trilayer, α is the angle defining the orientation of the in-plane magnetic field. (b) Cross section TEM photo for a Pt/NiO/YIG trilayer.

(H) is applied in-plane with angle α , and the resistance is detected by the standard four-probe method. Figure 1(b) shows a representative cross-section TEM picture for a Pt/NiO/YIG sample, which confirms a good thickness uniformity and clean interface.

Figure 2(a) shows the magnetoresistance (MR) measured in a Pt/NiO(2.5 nm)/YIG sample at field angle $\alpha = 0^\circ$ for various temperatures. The range of magnetic field over which the magnetoresistance occurs, coincides with that of the switching process of YIG [28]. The MR data for $T > 140$ K is consistent with the prediction $\rho_{\parallel} > \rho_{\perp}$ of the SMR theory. When $T = 140$ K, the MR nearly vanishes. For $T < 140$ K, a sign change of MR is observed and the MR amplitude increases with decreasing temperature. The MR data from the same sample at field angle $\alpha = 90^\circ$ is plotted in Fig. 2(b), which shows the same feature of the sign change. The SMR ratio $\Delta\rho_{\text{SMR}}/\rho_{xx}$ extracted from Fig. 2(a) and 2(b) are plotted in Fig. 2(c). The in-plane field angle dependence of Pt resistance $R_{xx}(400 \text{ Oe})$ at 300 K and 10 K is plotted in Fig. 2(d) and 2(e), which shows typical MR four fold symmetry consistent with Ref. [20]. Due to the insulating nature of YIG and NiO, the applied electric current flows only in the Pt layer. SMR is thus the only possible mechanism for the magnetoresistance in Pt on NiO/YIG, since Pt on the top of NiO has been proven to have negligible proximity-induced ferromagnetism [20], thus precluding the possibility of AMR. However, the sign change of the magnetoresistance in the low temperature regime seems to be at odds with SMR which, conventionally, can only be positive.

Fig. 3(a) shows the temperature dependence of the SMR ratio measured in Pt/NiO/YIG devices with different NiO thicknesses, d_{NiO} . The change in sign of the SMR occurs at higher temperatures in larger d_{NiO} samples. The d_{NiO} dependence proves to be a key piece of information for understanding the negative SMR. Furthermore, the SMR ratios have (positive) maxima at higher temperatures for thicker NiO samples. These d_{NiO} de-

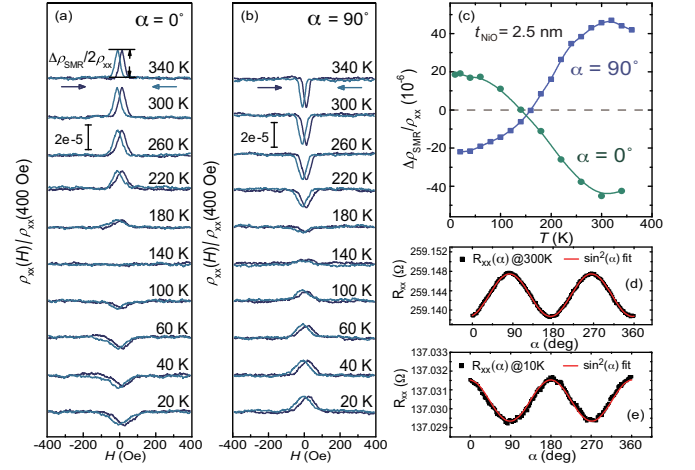


FIG. 2. (a),(b) Magnetoresistance measured for a Pt/NiO(2.5 nm)/YIG at $\alpha = 0^\circ$ and 90° for various temperatures. (c), Temperature dependence of the SMR ratio $\Delta\rho_{\text{SMR}}/\rho_{xx}$ for Pt/NiO(2.5 nm)/YIG at $\alpha = 0^\circ$ and 90° . (d), (e) In-plane field angle dependence of Pt film resistance at 300 K and 10 K with $|H| = 400$ Oe at which YIG is in-plane saturated.

pendent characteristics show a quantitative effect of the NiO on the SMR modulation, rather than a nuanced interface effect [29].

To gain further insight into the temperature dependence of spin transport in NiO, we carried out spin pumping measurements for the same samples, which can be regarded as the reciprocal process of the spin transport in the SMR measurement. Spin current is injected from YIG through NiO to generate a voltage in Pt via the inverse spin Hall effect (ISHE) [22]. The experimental setup is illustrated in Fig. 3(b): the Pt/NiO/YIG device is placed on a coplanar waveguide which serves as a 5 GHz microwave source. The microwave absorption spectrum (P) and the ISHE voltage (V_{ISHE}) are simultaneously obtained by a lock-in detection method in a magnetic field sweep.

Figure 3(c) is the microwave absorption spectrum for a Pt/NiO(2.7 nm)/YIG device at various temperatures, which shows that the ferromagnetic resonance induced absorption P_{abs} does not change much from 400 K to 20 K. However, V_{ISHE} detected at the same time, which is plotted in Fig. 3(d), shows a strong temperature dependence: V_{ISHE} is negligibly small at 20 K and increases quickly with increasing temperature to reach a maximum at 360 K. Similar temperature dependence can be found in all the Pt/NiO/YIG structures as shown in Fig. 3(e). In the low temperature limit the V_{ISHE} vanishes because the NiO becomes opaque to the spin current, consistent with our recent work [24]. The vanishing spin conductivity of NiO at low temperatures indicates the spin current generated from Pt cannot penetrate NiO to reach YIG, so the negative SMR at $T = 10$ K is not caused by the magnetic moment of the YIG layer.

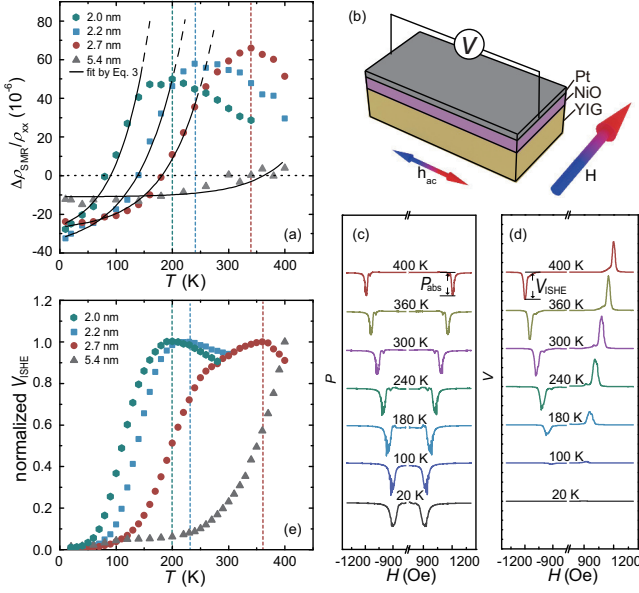


FIG. 3. (a), The SMR ratio measured in Pt/NiO(d_{NiO})/YIG devices with different NiO thickness d_{NiO} at various temperatures, which shows that the SMR sign change temperature is lower for a thinner NiO sample. The SMR ratio peak positions are marked by dashed lines. The black curves are the fitting based on Eq. (2). (b), The illustration for the spin pumping ISHE measurement for the Pt/NiO(d_{NiO})/YIG devices. (c), The microwave absorption spectrum measured in magnetic field scans at various temperatures for Pt/NiO(2.7 nm)/YIG, and P_{abs} is the microwave absorption due to the ferromagnetic resonance. (d), The ISHE signal measured at various temperatures for Pt/NiO(2.7 nm)/YIG. (e), V_{ISHE} in Pt/NiO/YIG devices versus temperature. The peak positions are marked by dashed lines, which are found to be close to the SMR ratio peak positions marked in Figure 2a.

Let us next provide an explanation for the negative SMR. The SMR in the trilayer system in this experiment is governed by the spin current through the Pt/NiO interface, which also reflects the effect of the presence of the NiO/YIG interface. The sign change and the thickness dependent behavior can be understood by assuming a ‘spin-flop’ coupling between NiO and YIG [27, 30], which means the antiferromagnetic axis (Néel vector unit \mathbf{n}_{AFM}) in NiO is perpendicular to the YIG magnetization unit vector \mathbf{m}_{FI} as illustrated in Fig. 4(a). Although a perpendicular coupling has not yet been confirmed experimentally for NiO on YIG, spin-flop coupling between NiO and other ferromagnets is quite common and well understood [27, 31, 32]. For the range of NiO thickness used here, the NiO is expected to be a single domain [33], and it coherently rotates with respect to the YIG magnetization when manipulated by the applied magnetic field. Thus, \mathbf{n}_{AFM} is always perpendicular to H below the Néel temperature, because the \mathbf{m}_{FI} is parallel to H . In the low temperature limit, e.g. 10 K, the spin current generated in Pt can not penetrate through the NiO, thus

the SMR signal is only caused by the NiO layer. The NiO local moments perpendicular to H gives rise to a 90-degree phase shift in the SMR field angular dependence with respect to the conventional SMR [9]. Such a 90-degree phase shift in a four-fold SMR field angular dependence is equivalent to a sign reversal in the conventional definition of MR, which explains the negative SMR in Pt/NiO/YIG at low temperatures.

At higher temperatures, but below the Néel point, antiferromagnetic order is maintained but the spin current from Pt has some transmission through NiO, which makes the effect of the YIG more visible as illustrated in Fig. 4(b). The negative SMR contribution from NiO and positive SMR contribution from YIG compete with each other. With increasing temperature, NiO becomes more transparent to the spin current, so the SMR contribution from YIG is enhanced. The SMR from NiO may also be suppressed because of the attenuation of the antiferromagnetic order at elevated temperatures. As a result, the zero point of the SMR occurs at a temperature where the antiferromagnet is still in the ordered phase. Thinner NiO layers have a lower Néel point due to the finite size effect [34], hence the SMR also changes the sign at lower temperatures in thinner-NiO samples, which is in accordance with our observation shown in Fig. 3(a).

Around the Néel point as illustrated in Fig. 4(c), the spin transparency of NiO are maximized [24], where the SMR contribution from YIG reaches its peak value and the SMR contribution from NiO vanishes. As explained above, all the main features of the SMR data in Pt/NiO/YIG, such as negative SMR at low temperatures, d_{NiO} dependent sign change temperature and peak temperature, can be interpreted by the ‘spin-flop’ configuration. Figure 4(d) shows an illustration of ρ_{SMR} temperature dependence, in which the temperature corresponding to these features are marked. We note that negative SMR has also been reported in bilayers of Pt on gadolinium iron garnet and Ar-sputtered YIG, in which the garnet interface moments can align perpendicularly to H [29, 35].

A simple phenomenological model based on the picture discussed above can provide not only a qualitative explanation for the SMR sign change, but also a quantitative description of the observed SMR temperature dependence. Let us consider a NM/AFM/FI trilayer system. The key assumption is that we can describe the spin current through the NM/AFM interface by

$$e\mathbf{j}_s = G_{\text{AF}}\mathbf{n}_{\text{AFM}} \times (\mathbf{n}_{\text{AFM}} \times \boldsymbol{\mu}_s) + t(T)\mathbf{m}_{\text{FI}} \times (\mathbf{m}_{\text{FI}} \times \boldsymbol{\mu}_s) = e\mathbf{j}_1 + e\mathbf{j}_2, \quad (1)$$

G_{AF} is the real part of the spin mixing conductance at NM/AFM interface. $\boldsymbol{\mu}_s$ is the spin accumulation at the same interface. The first term, which we denote by $e\mathbf{j}_1$, is what is expected for NM/AFM bilayer systems as seen in the case studied in Ref. [36]. We have introduced the

second term, which is denoted by $e\mathbf{j}_2$, to phenomenologically capture the effect of the FI layer. $t(T)$ encapsulates the temperature dependent transparency of the AFM to the spin current. In the case that the AFM is completely transparent the NM/FI bilayer result $\mathbf{m}_{\text{FI}} \times (\mathbf{m}_{\text{FI}} \times \boldsymbol{\mu}_s)$ is recovered. The linear combination of the NM/AFM and NM/FI terms has been chosen in an attempt to emulate our SMR data in the NM/AFM/FI system, seen

$$\frac{\delta\rho}{\rho_0} = \frac{2\theta_{\text{SHE}}^2\lambda_N^2}{d_N\sigma} \frac{G_{\text{AF}} \cos^2\phi_n + t(T) \cos^2\phi_m + \nu t(T) G_{\text{AF}} \sin^2(\phi_m - \phi_n)}{1 + \nu G_{\text{AF}} + \nu t(T) + \nu^2 t(T) G_{\text{AF}} \sin^2(\phi_m - \phi_n)} \tanh^2\left(\frac{d_N}{2\lambda_N}\right), \quad (2)$$

where we defined $\nu = (2\lambda_N/\sigma) \coth(d_N/\lambda_N)$ with λ_N and θ_{SHE} being the spin diffusion length and the spin Hall angle in NM, respectively, and $\sigma = \rho_0^{-1}$ is the conductivity of the NM layer. Here, $\phi_{n(m)}$ denotes the angle between $\mathbf{n}_{\text{AFM}}(\mathbf{m}_{\text{FI}})$ and the applied current \mathbf{j}_c in NM. Now we set out a hypothesis that the crossover between the negative and positive SMR is of the same origin as the temperature dependence of the spin pumping signal (Fig. 3(e)). In order to support it, the temperature dependence of $t(T)$ is obtained by fitting to the spin pumping data. The resulting function is then used alongside the other parameters in Eq. (1) to fit the SMR data. Fitting against two independent data sets, from SMR and spin pumping, poses a nontrivial test for the validity of our model.

Based on the observation that the ISHE signal in Fig. 3(e) is roughly exponential in the intermediate temperature regime, we focus our attention on demonstrating that a single parameter exponential function, $V_{\text{ISHE}} \propto t(T) \propto e^{aT} - 1$, can reproduce the temperature dependence of both spin pumping and SMR. We emphasize that this form of $t(T)$ has been chosen phenomenologically and is not expected to arise from any microscopic theory. The exponential behavior may not apply in the low-temperature regime as well as near the Néel temperature and the data points near and above the Néel temperature have been excluded from the fitting. Under these assumptions, a can be determined from the spin pumping data for each film thickness (TABLE I), generally with small errors.

We then fit $\delta\rho/\rho|_{\phi_m=0} - \delta\rho/\rho|_{\phi_m=\pi/2}$ based on Eq. (2) to the experimentally obtained SMR ratio $\Delta\rho_{\text{SMR}}/\rho_{xx}$ in Fig. 3(a) using the fitted value of a from the V_{ISHE} data. We fix $\lambda_N = 1.5\text{nm}$, $d_N = 4.0\text{nm}$, $\rho_0 = \sigma^{-1} = 860\ \Omega\text{nm}$, and $\theta_{\text{SHE}} = 0.05$, which are taken to be relevant values to the present experiment, and we further determine G_{AF} and G_F from the data, where the latter two are defined by $t(T) = G_F(e^{aT} - 1)$, $\phi_n - \phi_m = \pi/2$, respectively. The temperature dependence of ρ_0 and θ_{SHE} is ignored since they scale in some powers of T , which is wiped

in Fig. 3(a), which seems to indicate a crossover from NM/AFM bilayer like behavior at low temperatures to NM/FI bilayer like behavior for higher temperatures.

Once we admit the form of the interfacial spin current in Eq. (1), we can calculate the SMR by employing the diffusion equation and the Onsager principle, according to Refs. [10, 36]. The SMR contribution to the longitudinal resistivity then is given by

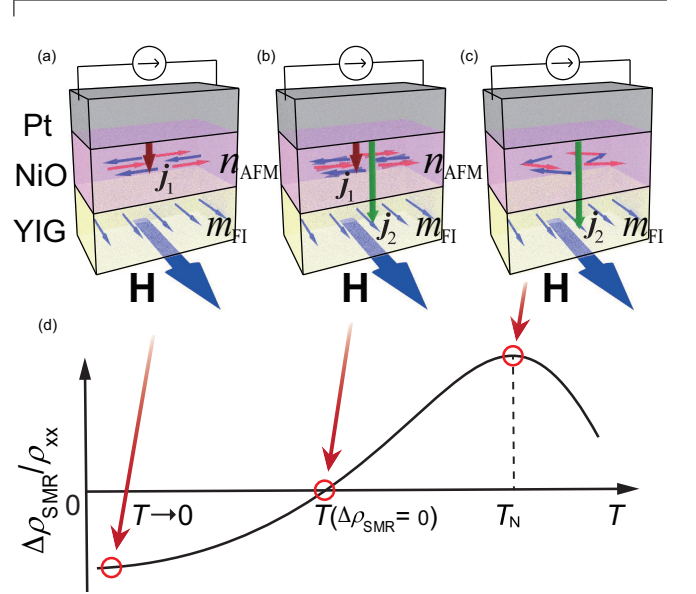


FIG. 4. Illustrations for the magnetic structure and spin transport in Pt/NiO/YIG at different temperatures. The red and green arrows represent the phenomenologically described spin currents, \mathbf{j}_1 and \mathbf{j}_2 in Eq. (1), respectively. The length of the arrow describes the penetration depth of the spin current. (a), T close to the low temperature limit. (b), T far above the low temperature limit and lower than the Néel temperature. (c), T higher than the Néel temperature. (d), Illustration of T -dependent SMR in which the temperatures corresponding to the conditions in Fig. 4(a), (b) and (c) are marked with red circle.

out by the exponential change in $t(T)$. The results are summarized in TABLE I, as well as shown in Fig. 3(a) by solid lines. The deviation of the data points from the lines is small and the fitting is satisfactory. G_{AF} is relatively insensitive to d_{NiO} which is also consistent with the observation made in Ref. [37] that only the first few layers of NiO should contribute to spin-mixing conductance. To discuss the values of a and G_F requires a microscopic understanding of $t(T)$, which we lack at present. Nevertheless, one can read a clear correlation between SMR and spin pumping, which provides another

d_{NiO}	$a[K^{-1}]$	G_{AF}	G_F
2.0	$1.83 \pm 0.22 \times 10^{-2}$	$3.58 \pm 0.32 \times 10^{12}$	$8.39 \pm 0.57 \times 10^{11}$
2.2	$1.38 \pm 0.19 \times 10^{-2}$	$4.48 \pm 0.17 \times 10^{12}$	$7.78 \pm 0.26 \times 10^{11}$
2.7	$1.42 \pm 0.10 \times 10^{-2}$	$3.67 \pm 0.09 \times 10^{12}$	$3.01 \pm 0.08 \times 10^{11}$
5.4	$1.44 \pm 0.02 \times 10^{-2}$	$1.51 \pm 0.15 \times 10^{12}$	$0.08 \pm 0.01 \times 10^{11}$

TABLE I. The results of the fitting with the data from the SMR and spin pumping signals. The parameters are defined in the main text. The units of the last two columns are both $[\Omega^{-1}\text{m}^{-2}]$.

strong evidence for the spin conductive property of NiO. It should be emphasized that the spin current injection from Pt to NiO cannot be explained by spin transfer torque; the latter is taken into account by the first term in Eq. (1) and is unable to explain the presence of the second term. This result implies that the spin transport through AFM is mainly driven by incoherent fluctuations of the magnetic moments, and calls for a comprehensive theory that can handle spin-pumping and SMR at the same time.

Our result highlights the importance of magnetic structure in AFM for spin transport, which suggests an alternative degree of freedom of spin manipulation. This work also indicates that the SMR measurement in Pt/AFM/FI structures can be used to study the coupling between AFM and FI.

This work was supported by ERATO “Spin Quantum Rectification”, Grant-in-Aid for Scientific Research on Innovative Area, “Nano Spin Conversion Science” (26103005) from MEXT, Japan, NEC corporation and World Premier International Research Center Initiative (WPI) all from MEXT, Japan, and NEC corporation. A part of this work was performed under the Inter-university Cooperative Research Program of the Institute for Materials Research, Tohoku University (Proposal No.15K0089). K. Y. is supported by the JSPS Grant-in-Aid for Scientific Research No.26-1204.

* qiuzy@imr.tohoku.ac.jp

- [1] I. A. Campbell, A. Fert, and O. Jaoul, *J. Phys. C* **3**, S95 (1970).
- [2] T. McGuire and R. Potter, *IEEE Trans. Magn.* **11**, 1018 (1975).
- [3] G. Binasch, P. Grünberg, F. Saurenbach, and W. Zinn, *Phys. Rev. B* **39**, 4828 (1989).
- [4] M. N. Baibich, J. M. Broto, A. Fert, F. N. Van Dau, F. Petroff, P. Etienne, G. Creuzet, A. Friederich, and J. Chazelas, *Phys. Rev. Lett.* **61**, 2472 (1988).
- [5] M. Julliere, *Phys. Lett. A* **54**, 225 (1975).
- [6] T. Miyazaki and N. Tezuka, *Journal of Magnetism and Magnetic Materials* **139**, L231 (1995).
- [7] S. Yuasa, T. Nagahama, A. Fukushima, Y. Suzuki, and K. Ando, *Nat. Mater.* **3**, 868 (2004).
- [8] S. S. P. Parkin, C. Kaiser, A. Panchula, P. M. Rice, B. Hughes, M. Samant, and S.-H. Yang, *Nat. Mater.* **3**, 862 (2004).
- [9] H. Nakayama, M. Althammer, Y.-T. Chen, K. Uchida, Y. Kajiwara, D. Kikuchi, T. Ohtani, S. Geprägs, M. Opel, S. Takahashi, R. Gross, G. E. W. Bauer, S. T. B. Goennenwein, and E. Saitoh, *Phys. Rev. Lett.* **110**, 206601 (2013).
- [10] Y.-T. Chen, S. Takahashi, H. Nakayama, M. Althammer, S. T. B. Goennenwein, E. Saitoh, and G. E. W. Bauer, *Phys. Rev. B* **87**, 144411 (2013).
- [11] M. Althammer, S. Meyer, H. Nakayama, M. Schreier, S. Altmannshofer, M. Weiler, H. Huebl, S. Geprägs, M. Opel, R. Gross, D. Meier, C. Klewe, T. Kuschel, J.-M. Schmalhorst, G. Reiss, L. Shen, A. Gupta, Y.-T. Chen, G. E. W. Bauer, E. Saitoh, and S. T. B. Goennenwein, *Phys. Rev. B* **87**, 224401 (2013).
- [12] M. Weiler, M. Althammer, M. Schreier, J. Lotze, M. Pernpeintner, S. Meyer, H. Huebl, R. Gross, A. Kamra, J. Xiao, Y.-T. Chen, H. Jiao, G. E. W. Bauer, and S. T. B. Goennenwein, *Phys. Rev. Lett.* **111**, 176601 (2013).
- [13] S. Meyer, M. Althammer, S. Geprägs, M. Opel, R. Gross, and S. T. B. Goennenwein, *Applied Physics Letters* **104**, 242411 (2014).
- [14] R. Iguchi, K. Sato, D. Hirobe, S. Daimon, and E. Saitoh, *Applied Physics Express* **7**, 013003 (2014).
- [15] M. Schreier, T. Chiba, A. Niedermayr, J. Lotze, H. Huebl, S. Geprägs, S. Takahashi, G. E. W. Bauer, R. Gross, and S. T. B. Goennenwein, *Phys. Rev. B* **92**, 144411 (2015).
- [16] J. Lotze, H. Huebl, R. Gross, and S. T. B. Goennenwein, *Phys. Rev. B* **90**, 174419 (2014).
- [17] S. R. Marmion, M. Ali, M. McLaren, D. A. Williams, and B. J. Hickey, *Phys. Rev. B* **89**, 220404 (2014).
- [18] M. Isasa, A. Bedoya-Pinto, S. Vlez, F. Golmar, F. Sanchez, L. E. Hueso, J. Fontcuberta, and F. Casanova, *Applied Physics Letters* **105**, 142402 (2014).
- [19] C. O. Avci, K. Garello, A. Ghosh, M. Gabureac, S. F. Alvarado, and P. Gambardella, *Nat Phys* **11**, 570 (2015).
- [20] T. Shang, Q. F. Zhan, H. L. Yang, Z. H. Zuo, Y. L. Xie, L. P. Liu, S. L. Zhang, Y. Zhang, H. H. Li, B. M. Wang, Y. H. Wu, S. Zhang, and R.-W. Li, *Applied Physics Letters* **109**, 032410 (2016).
- [21] C. Hahn, G. de Loubens, V. V. Naletov, J. B. Youssef, O. Klein, and M. Viret, *EPL (Europhysics Letters)* **108**, 57005 (2014).
- [22] H. Wang, C. Du, P. C. Hammel, and F. Yang, *Phys. Rev. Lett.* **113**, 097202 (2014).
- [23] T. Moriyama, S. Takei, M. Nagata, Y. Yoshimura, N. Matsuzaki, T. Terashima, Y. Tserkovnyak, and T. Ono, *Applied Physics Letters* **106**, 162406 (2015).
- [24] Z. Qiu, J. Li, D. Hou, E. Arenholz, A. T. N'Diaye, A. Tan, K.-i. Uchida, K. Sato, S. Okamoto, Y. Tserkovnyak, Z. Q. Qiu, and E. Saitoh, *Nature Communications* **7**, 12670 (2016).
- [25] L. Frangou, S. Oyarzún, S. Auffret, L. Vila, S. Gambarelli, and V. Baltz, *Phys. Rev. Lett.* **116**, 077203 (2016).
- [26] W. Lin, K. Chen, S. Zhang, and C. L. Chien, *Phys. Rev. Lett.* **116**, 186601 (2016).
- [27] N. C. Koon, *Phys. Rev. Lett.* **78**, 4865 (1997).
- [28] K. Uchida, Z. Qiu, T. Kikkawa, R. Iguchi, and E. Saitoh, *Applied Physics Letters* **106**, 052405 (2015).

- [29] S. Vélez, A. B. Pinto, W. Yan, L. E. Hueso, and F. Casanova, arXiv:1606.02968.
- [30] T. Schulthess and W. Butler, Physical Review Letters **81**, 4516 (1998).
- [31] I. P. Krug, F. U. Hillebrecht, M. W. Haverkort, A. Tanaka, L. H. Tjeng, H. Gomonay, A. Fraile-Rodríguez, F. Nolting, S. Cramm, and C. M. Schneider, Phys. Rev. B **78**, 064427 (2008).
- [32] J. Li, A. Tan, S. Ma, R. F. Yang, E. Arenholz, C. Hwang, and Z. Q. Qiu, Phys. Rev. Lett. **113**, 147207 (2014).
- [33] W. Kim, E. Jin, J. Wu, J. Park, E. Arenholz, A. Scholl, C. Hwang, and Z. Q. Qiu, Phys. Rev. B **81**, 174416 (2010).
- [34] D. Alders, L. Tjeng, F. Voogt, T. Hibma, G. Sawatzky, C. Chen, J. Vogel, M. Sacchi, and S. Iacobucci, Physical Review B **57**, 11623 (1998).
- [35] K. Ganzhorn, J. Barker, R. Schlitz, B. A. Piot, K. Ollefs, F. Guillou, F. Wilhelm, A. Rogalev, M. Opel, M. Althammer, S. Geprägs, H. Huebl, R. Gross, G. E. W. Bauer, and S. T. B. Goennenwein, Phys. Rev. B **94**, 094401 (2016).
- [36] S. Takei, B. I. Halperin, A. Yacoby, and Y. Tserkovnyak, Phys. Rev. B **90**, 094408 (2014); Y.-T. Chen, S. Takahashi, H. Nakayama, M. Althammer, S. T. B. Goennenwein, E. Saitoh, and G. E. W. Bauer, Journal of Physics: Condensed Matter **28**, 103004 (2016).
- [37] R. Cheng, J. Xiao, Q. Niu, and A. Brataas, Phys. Rev. Lett. **113**, 057601 (2014).